

FrameFusion: Combining Similarity and Importance for Video Token Reduction on Large Visual Language Models

Tianyu Fu^{*1,2}, Tengxuan Liu^{*1,2}, Qinghao Han^{*3},
Guohao Dai^{4,2}, Shengen Yan², Huazhong Yang¹, Xuefei Ning¹, Yu Wang¹
¹Tsinghua University ²Infinigence-AI ³Peking University ⁴Shanghai Jiao Tong University

Abstract

The increasing demand to process long and high-resolution videos significantly burdens Large Vision-Language Models (LVLMs) due to the enormous number of visual tokens. Existing token reduction methods primarily focus on importance-based token pruning, which overlooks the redundancy caused by frame resemblance and repetitive visual elements. In this paper, we analyze the high vision token similarities in LVLMs. We reveal that token similarity distribution condenses as layers deepen while maintaining ranking consistency. Leveraging the unique properties of similarity over importance, we introduce FrameFusion, a novel approach that combines similarity-based merging with importance-based pruning for better token reduction in LVLMs. FrameFusion identifies and merges similar tokens before pruning, opening up a new perspective for token reduction. We evaluate FrameFusion on diverse LVLMs, including Llava-Video-{7B,32B,72B} and MiniCPM-V-8B, on video understanding, question-answering, and retrieval benchmarks. Experiments show that FrameFusion reduces vision tokens by 70%, achieving $3.4 - 4.4\times$ LLM speedups and $1.6 - 1.9\times$ end-to-end speedups, with an average performance impact of less than 3%. Our code is available at <https://github.com/thu-nics/FrameFusion>.

1. Introduction

Large Vision-Language Models (LVLMs) have shown outstanding abilities across various video understanding scenarios, including temporal and spatial perception, recognition, and reasoning [4, 14, 29, 34]. Growing applications also demand LVLMs’ ability to process longer and more complex videos [18, 21, 24].

However, video understanding incorporates substantial computing overhead for LVLMs. Common LVLMs sample frames from the video, split each into image patches, and then sequentially embed them as vision tokens with a visual

*Equal contribution.

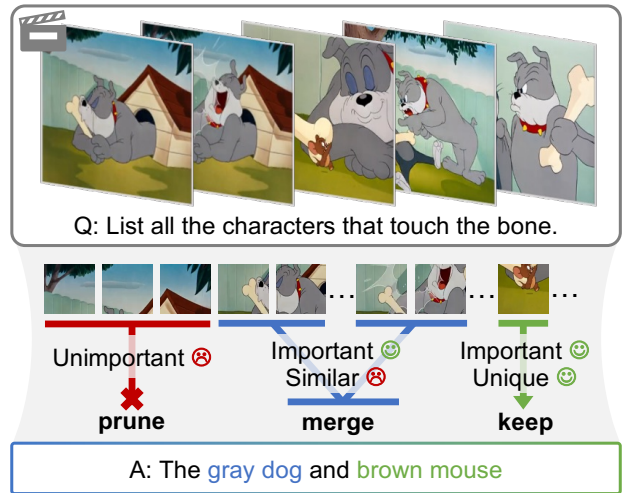


Figure 1. The central idea of FrameFusion. Compared with importance-based token pruning, FrameFusion additionally applies similarity-based token merging, keeping only important and unique vision tokens.

encoder. Though effective, it requires the processing of a huge amount of vision tokens for LVLMs. Take Google Gemini as an example, with the standard sampling rate of 1 frame per second (fps), it requires an astonishing amount of one million tokens to understand an hour’s video [21].

The importance-based token pruning has been extensively explored by previous works to solve the efficiency problem. They reduce vision tokens with various importance matrices, like accumulative attention score [7, 23, 35] and L2-norm of token feature [3]. However, there exist extensive important yet similar vision tokens in LVLMs due to frame resemblance and similar visual elements, while the effect of these tokens is less explored.

In this work, we recover similarity as a perpendicular property to importance for vision tokens reduction. The main idea is that although some frames are important for visual understanding, their high similarity leads to redundant information. These similar tokens, like those alike im-

age patches from adjacent frames, hardly provide additional information, thus can be merged. To fully harness the potential of similarity-based merging, we study the token similarity distribution of LVLMs by answering three questions:

1. Where and when does similarity appear?
2. What is the value distribution of token similarity?
3. How consistent is the ranking of token similarity across layers?

Based on the observations, we propose FrameFusion to combine both similarity and importance for efficient LVLM token reduction. FrameFusion first evaluates the token similarity with minimum overhead and progressively merges similar tokens. After the similarity-based merging, FrameFusion then utilizes importance-based pruning to reduce tokens to the given computing budget.

Our contributions are three-folds:

1. We analyze the characteristics of token similarities across input positions and layers of LVLM.
2. We propose FrameFusion to hierarchically merge similar vision tokens and prune unimportant ones in a plug-and-play manner.
3. We conduct extensive experiments to show the effectiveness of FrameFusion on various video tasks.

Experiments show that FrameFusion pushes the Pareto front further for token compression. It successfully reduces the token budget and computing FLOPs to 30%, while maintaining comparable performance with the original dense model. The simple yet effective design helps FrameFusion to generalize across various model sizes, input lengths, and video tasks.

2. Related Work

2.1. Large Vision Language Model (LVLMs)

The LVLM architecture typically consists of a vision encoder and a Large Language Model (LLM) [4, 13, 14, 18, 24, 29, 34]. The vision encoder converts visual inputs into token sequences, which the LLM then processes alongside text sequences to generate responses. Specifically, for video input, frames are first sampled temporally and then specially divided into sequences of image patches before sending to the vision encoder [14, 29, 34], as shown in Figure 1. Due to the high temporal and spatial resolution demands of complex video understanding tasks, token lengths can reach up to one million for an hour-long video [21], imposing significant computational overhead on LVLMs.

2.2. Token Compression

Motivated by the heavy overhead of video processing, token compression becomes an essential method for LVLM efficiency. Existing methods compress tokens at three subsequent processes.

The first branch of work reduces the initial visual inputs

before sending them to the vision encoder. They set rules to mix different temporal sampling frequencies [28, 34] and special resolutions [5, 29] when converting videos to input sequences, introducing trade-offs between visual detail and efficiency. Despite the simplicity, they inevitably incur direct detail losses and neglect the visual content guidance during compression.

Other works reduce tokens inside the vision encoder. They selectively retrieve [11] or condense [18] vision tokens in the vision encoder based on the guidance of text instructions. Yet, they require re-encoding all vision tokens if the text instruction changes, which incurs significant overheads for common multi-round conversation scenarios. Besides, an additional model fine-tuning is often needed to align the new vision encoding space.

Another branch of work focuses on token reduction in the subsequent LLM. For text-only tasks, previous works design static [8, 10, 26] or dynamic [9, 12, 19, 35] pruning pattern based on the importance of token (or KV-Cache). Emerging concurrent works highlight the specific token importance distribution for vision-language tasks [2, 16, 22, 31, 33], which further increase the sparsity of importance-based token pruning. However, as shown in Figure 4, token importance is inconsistent across different layers. It incurs prediction loss by pruning an unimportant token at shallow layers, which becomes important but inaccessible at deeper layers. FrameFusion falls in this category, exploring a more consistent and perpendicular token reduction method: similarity-based token merging.

3. Token Similarity Analysis

While token importance properties of LVLMs have been extensively studied [2, 16, 22, 33], a thorough and comparative analysis of token similarity remains lacking. Thus, we conduct oracle experiments to answer three key questions regarding the characteristics of token similarity, comparing them with token importance.

3.1. Experiment Setups and Notion Definitions

In this section, we present the oracle results with the Llava-Video-7B [34] model tested on 128 video samples (64 frames at 1 fps) from the comprehensive VideoMME [6] datasets. All metrics are averaged over all test samples unless otherwise noted. Results on different models are similar and provided in Appendix 10.2.

We define token importance and similarity using the notations $I^{(l)} \in \mathbb{R}^N$ and $S^{(l)} \in \mathbb{R}^N$, respectively, where l indicate the layer index of the LLM. For clarity, we omit l where it does not introduce ambiguity. We use the subscript t to index the token along the input length dimension N . The token features at layer l are represented as $\mathbf{X}^l \in \mathbb{R}^{N \times d}$.

Following previous works [2, 35], the token importance $I_t^{(l)}$ is quantified using the cumulative attention score, cal-

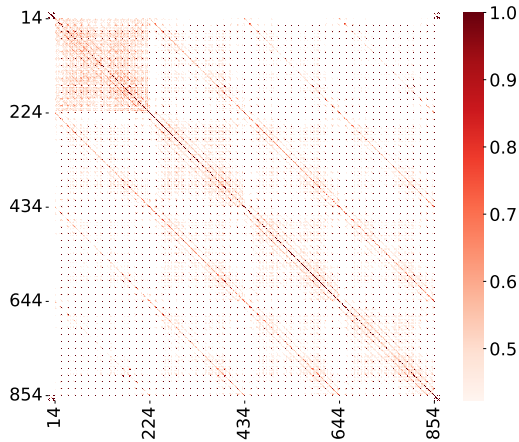


Figure 2. Token similarities among all input tokens at the first LLM layer in Llava-Video-7B models. For visual clarity, the color bar displays only the top 90% of similarity values. Vision tokens begin at index 14, with 210 tokens per frame.

culated by summing the post-softmax attention scores vertically across the t -th column and averaging this sum across all attention heads at layer l .

For token similarity $S_t^{(l)}$, we specifically define it as the cosine similarity between a vision token and its corresponding token from the preceding frame. The rationale for this definition is detailed in Section 3.2. Formally, if each frame is encoded into P vision tokens, token similarity is calculated using the following equation:

$$S_t = \frac{X_{t-P}^T X_t}{\|X_{t-P}\|_2 \cdot \|X_t\|_2} \quad (1)$$

3.2. Where and When Does Similarity Appear?

We first investigate which tokens are most likely to demonstrate high similarity, as these are expected to have a greater potential for merging. To ensure figure clarity within the limited resolution, we limit the number of frames so that each input sequentially consists of 14 system prompt tokens, 840 vision tokens (representing 4 frames at 210 tokens per frame), and 20 user instruction tokens. Figure 2 displays the $N \times N$ cosine similarity matrix for all input tokens at the first LLM layer. A prominent 210th sub-diagonal appears, reflecting high similarities between tokens i and $i + P$, where $P = 210$ corresponds to the number of vision tokens per frame. This pattern underscores our initial observation:

Observation 1. Spatially corresponding vision tokens between adjacent temporal frames exhibit higher cosine similarities than other token pairs.

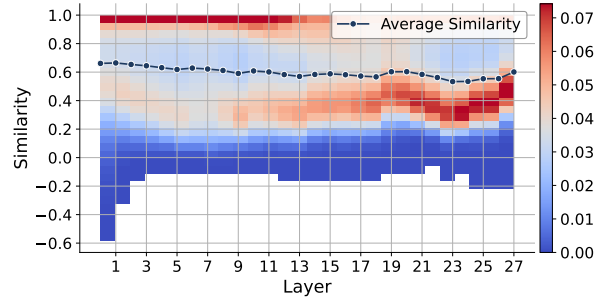


Figure 3. Heatmap of token similarity across different model layers. Each cell represents a similarity range at a specific layer, with color intensity denoting distribution frequency. The line overlay shows the average token similarity at each layer.

Based on this observation, we focus on token similarities among these particular tokens and define token similarity as described in Equation 1. It is also worth noting that similar to token importance, the similarities between vision-language tokens are significantly lower than those between vision-vision or language-language tokens. This finding motivates a similar design choice to separate token compression for vision and language tokens, as proposed in prior work [2].

3.3. What Is the Distribution of Token Similarity?

To decide the appropriate way for token compression, we explore the distribution of token similarities across different layers. As illustrated in Figure 3, although the average token similarity across layers remains relatively stable, there is a significant shift in the distribution of these similarities:

Observation 2. High token similarities exhibit an obvious reduction in deeper model layers.

This trend is further confirmed by the variance in token similarity, which decreases from 6.0×10^{-2} at the first layer to 3.7×10^{-2} at the last layer. It illustrates a tightening of the distribution, with more numerical details in Appendix 10.1.

The causal attention mechanism in LLMs contributes to this shift, where later vision tokens can aggregate information from earlier tokens, but not vice versa. The attention range differences lead to a divergence in the similarity of tokens that were initially similar, such as corresponding tokens from adjacent frames. This divergence accumulates as layers deepen.

Based on this observation, FrameFusion prioritizes token merging at shallower layers rather than deeper layers to fully utilize the polarized high similarities.

3.4. How Consistent Is the Ranking of Token Similarity Across Layers?

The ranking consistency of token properties guides the compression strategy designs. For importance-based token

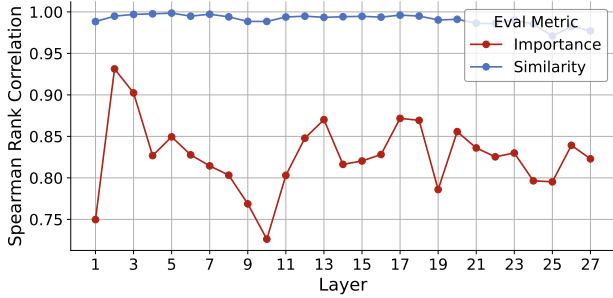


Figure 4. Spearman Rank Correlation between adjacent layers for the Llava-Video-7B model.

pruning, the consistency across layers determines whether tokens deemed unimportant at shallow layers might become important at deeper layers. Early works [2, 23] adopt cascaded token pruning, where pruned tokens are no longer accessible in subsequent layers. These methods prioritize efficiency by eliminating token computations in both attention and Feed Forward Network (FFN) modules, and the importance is only computed once for pruned tokens. In contrast, more recent works [17, 20, 35] adopt non-cascaded pruning, which maintains the accessibility of all tokens across all layers by only pruning the KV-Cache at the attention layer. Yet, these methods do not reduce computation for the FFN and incur higher costs due to the need to compute importance for all tokens at every layer. Previous researches [8, 25] highlight the inconsistency of token importance across layers, which justifies re-evaluating pruning decisions at each layer. However, does a similar conclusion hold for token similarity?

To quantitatively assess the ranking consistency of token importance and token similarity, we calculate their respective Spearman Rank Correlations (SRC) [30] between adjacent layers. The SRC measures the degree to which the ranking of metrics in one layer correlates with the rankings in other layers. As shown in Figure 4, the SRCs for token similarity approach 1 across layers, indicating consistent ordering. In contrast, the SRCs for token importance are consistently lower, indicating weaker consistency across layers. We observe the following:

Observation 3. Token similarity demonstrates high rank consistency across different model layers.

Combining Observations 2 and 3, we conclude an interesting phenomenon: although the token similarity distribution condenses as layers deepen, tokens with the highest similarities remain the most similar. Motivated by this high consistency in similarity, FrameFusion employs similarity-based merging in a cascaded manner. Once highly-similar tokens are merged at shallow layers, they are not separated in subsequent computations.

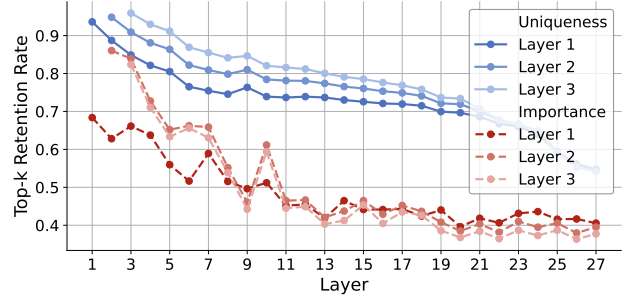


Figure 5. The Top-30% retention rate across model layers using different retention metrics and starting layers.

We further validate this cascaded design choice by quantifying the top-k retention rate across model layers. For notion simplicity, we define token uniqueness as 1 minus similarity. To calculate the top-k retention rate, we identify the set of top-k tokens under token uniqueness or importance metrics at each layer. The top-k retention rate for layer l , starting from layer i , is defined as the intersection rate between the top-k tokens from both layers l and i .

To formalize the calculation of the top-k retention rate, we denote the set of indices of the top-k retaining tokens based on the scoring function $f : \mathbb{R}^{N \times d} \rightarrow \mathbb{R}^N$ at layer l as follows:

$$T^{(l)} = \left\{ i \mid i \in \text{Top-K}(f(\mathbf{X}^{(l)})) \right\}, \quad (2)$$

where scoring function f can be token importance or token similarity, $\text{Top-K} : \mathbb{R}^N \rightarrow \mathbb{N}^K$ function returns the indices of the top-k values. The top-k retention rate $R_i^{(l)}$ of layer l with the starting layer i is calculated as:

$$R_i^{(l)} = |T^{(l)} \cap T^{(i)}| / |T^{(i)}|. \quad (3)$$

As shown in Figure 5, we quantify the top-30% retention rate with shallow starting layers 0 to 2 under different metrics. The token similarity exhibits a much higher retention rate than token importance. This finding validates the superiority of using token similarity over importance for cascaded token pruning, achieving a better accuracy trade-off.

4. FrameFusion Design

Building upon the observations from Section 3, we introduce FrameFusion, a novel token compression technique for video LVLMs, exploring a new perspective of token similarity. The design of FrameFusion is detailed in Section 4.1, followed by an explanation of the rationale behind each key design choice in Section 4.2.

4.1. Two-Stage Token Compression

The core concept of FrameFusion is illustrated in Figure 1: unlike traditional methods that primarily employ

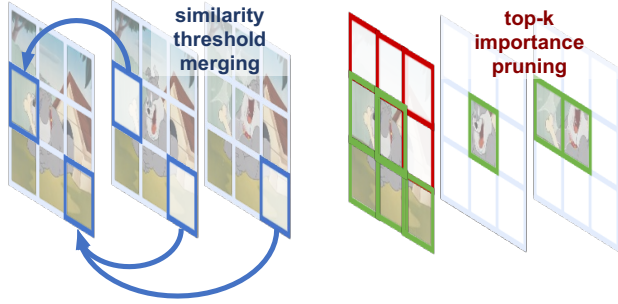


Figure 6. FrameFusion first merges tokens with similarities above a specified threshold at shallow layers, then applies top- k importance pruning to comply with the given computational constraints.

importance-based token pruning, FrameFusion also emphasizes similarity-based token merging. It merges similar tokens and prunes unimportant ones, retaining only those that are both important and unique. The two-stage token reduction process of FrameFusion is shown in Figure 6.

Merging stage. In the initial merging stage, FrameFusion utilizes token similarity to merge vision tokens. It computes the token similarity $S^{(l)}$ at the current layer using Equation 1, where only N cosine similarities are computed between the corresponding vision tokens of adjacent frames. Tokens that exceed the similarity threshold $S_{\text{threshold}}$ are grouped with their analogous tokens from the previous frame. These merging groups are transitive, allowing concatenated groups to form a larger group containing more than two tokens as shown in Figure 6. Within each group, FrameFusion performs element-wise averaging of all tokens, assigning the result to the first token in the group. This forward merging strategy ensures that subsequent vision tokens can still aggregate information from all preceding tokens using causal attention.

The merging stage is applied across successive shallow LLM layers to progressively merge similar tokens, until the number of similar tokens falls below the threshold $N_{\text{threshold}}$ at a specific layer. Merging occurs right before the FFN module; however, to reduce the number of tokens for the attention module at the first LLM layer, an additional merging step is performed before it. After the merging stage, the remaining unique tokens advance to the pruning stage.

Pruning stage. After the merging stage, FrameFusion further prunes unimportant tokens. As discussed in Section 3.1, FrameFusion uses cumulative attention scores to represent token importance. Based on a user-defined computational cost budget, FrameFusion calculates the maximum number of remaining tokens k that fits within the budget. It then applies top- k importance pruning to retain only the important tokens from the remaining unique ones.

Through the merging and pruning stages, only the unique and important vision tokens are retained for subsequent pro-

cessing, significantly boosting LVLm efficiency.

4.2. Design Choice Rationales

In this subsection, we explain the key design choices of FrameFusion with rationales from key observations in Section 3.

Unlike token importance, which reuses the existing $N \times N$ attention scores, token similarity introduces a new, orthogonal metric. To avoid additional $N \times N$ similarity computations for all token pairs, we leverage Observation 1 to compute only empirically similar token pairs with an $O(N)$ complexity:

Design Choice 1. FrameFusion computes token similarities only between corresponding vision tokens of adjacent frames.

Another key design choice is determining the layers at which to perform token reduction. For importance-based pruning, previous study [2] observes the reduction in vision token importance after the initial two layers for LVLms. Thus, it advises applying importance-based pruning after the second layer. Other works also confirm the accuracy advantage of aggressive pruning only at deeper layers [1, 8]. In contrast, merging relies on high token similarities and therefore prefers shallow layers, according to Observation 2. Based on the contradictory preferences of similarity-based merging and importance-based pruning, FrameFusion is designed as follows:

Design Choice 2. FrameFusion applies token merging at the initial successive layers, then pruning at a later layer.

The final key design choice is whether merged tokens should remain reduced in subsequent layers, i.e., whether to use cascaded token merging. This choice depends on whether tokens merged in shallow layers are likely to be needed in deeper layers. Given the high rank consistency and retention rate of token similarities discussed in Observation 3, we adopt the following design to achieve a better efficiency trade-off:

Design Choice 3. FrameFusion merges tokens in a cascaded manner.

These rationales for the three key design choices in FrameFusion enhance the explainability of its better performance.

5. Experiment

5.1. Setups

Baselines. We compare FrameFusion with state-of-the-art token pruning baselines, StreamingLLM [26] and FastV [2]. Hyperparameters follow the official implementations and are detailed in Appendix 7.

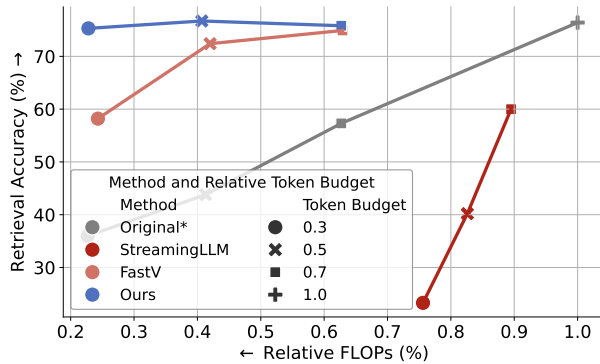


Figure 7. The accuracy-computation trade-offs of various token compression methods, tested on Llava-Video-7B with VideoNIAH benchmark. Original* represents the original model with reduced frame rates.

Token Budget. We term the *token budget* as the average number of tokens required for the KV-Cache at the start of the decoding stage. The *relative token budget*, denoted as C , is the token budget of compression methods divided by the original input length N . The relative token budget approximates the relative KV-Cache utilization for each compression method. We set $C = 30\%$ for all token compression methods if not specified. Specifically, for the cascaded methods FrameFusion and FastV, the token budget equals the average token length per layer across both the prefill and decode stages. For StreamingLLM, the token budget equals the token length in KV-Cache at the decode stage, which also equals the attention span during the prefill stage.

Models. We evaluate our approach on widely used video LLMs, including Imms-lab models: LLaVA-Video-{7B,72B}-Qwen2 (referred to as Llava-Video-{7B,72B}), LLaVA-NeXT-Video-32B-Qwen (referred to as Llava-Video-32B) [34], and the openbmb model MiniCPM-V-2.6 (referred to as MiniCPM-V-8B) [29].

Benchmarks. We use Imms-eval [32] as the primary evaluation framework to test diverse video benchmarks, including VideoMME [6] for video understanding, NEX-TQA [27] for video question-answering, and Video Needle In A Haystack (VideoNIAH)[36] for visual content retrieval.

5.2. Accuracy-Computation Trade-off

As shown in Figure 7, we explore the accuracy-computation trade-off of different token compression methods. The relative FLOPs is normalized by the original dense model with the video sampling rate at 1 frame per second. For the original* variant, the relative FLOPs is altered by directly multiplying the sampling rate with the relative token budget. FrameFusion advances the Pareto Front in video content retrieval accuracy and computing FLOPs across varied relative token budgets.

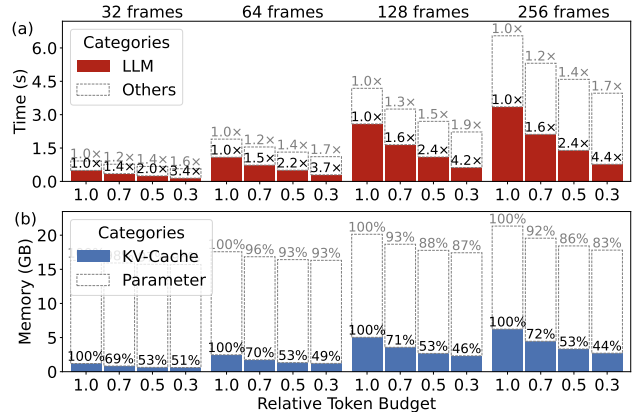


Figure 8. Runtime and memory breakdown of Llava-Video-7B on a single A100-80GB GPU using FrameFusion. A relative token budget of 1.0 represents the original dense model. Numbers on bars show (a) LLM and end-to-end speedups and (b) LLM’s KV-Cache and total relative memory.

5.3. Performance

FrameFusion outperforms state-of-the-art token compression methods across various models and benchmarks, achieving performance comparable to the dense model at a 30% token budget (Table 1). Additional results for additional budgets are in Appendix 8.1. Across VideoMME, NEX-TQA, and VideoNIAH benchmarks, FrameFusion limits its relative performance drops to under 3%. In contrast, StreamingLLM and FastV show drops of up to 13% and 7% for VideoMME and NEX-TQA, and 70% and 24% for VideoNIAH. Further retrieval performance details are in Appendix 8.2.

5.4. Efficiency

We evaluate efficiency on a single NVIDIA A100-80GB GPU, averaging results over 128 videos from the VideoMME benchmark. Figure 8 highlights how FrameFusion improves runtime and memory efficiency for the colored components.

Time. FrameFusion achieves 3.4-4.4 \times speedups with a 30% token budget across various input frames. Including other runtimes like ViT and CPU calls, FrameFusion maintains 1.6 – 1.9 \times end-to-end speedups. Speedup results for additional model sizes are provided in Appendix 8.3.

Memory. FrameFusion reduces LLM memory consumption for KV-Cache and corresponding activations (noted as “KV-Cache” in Figure 8) to 44% – 51% with a 30% token budget, enabling more frames to fit within GPU memory limits.

5.5. Scalability

Scaling Model Size. We test the scalability of FrameFusion across diverse model parameter sizes with the Llava-Video

Model	Method	VideoMME \uparrow			NExt-QA \uparrow		VideoNIAH \uparrow			Avg.
		Short	Medium	Long	Multi Choice	Open End	Edit	Insert1	Insert2	
Llava-Video-7B	Original	75.8	61.7	52.2	83.2	32.1	90.7	50.7	88.0	66.8
	StreamingLLM	63.4	54.1	46.4	79.0	30.3	26.0	15.3	28.7	42.9
	FastV	68.4	58.0	49.6	81.1	31.2	69.3	28.7	76.7	57.9
	Ours	74.0	59.8	50.0	81.8	31.7	90.0	48.7	87.3	65.4
MiniCPM-V-8B	Original	69.1	56.6	49.8	78.9	13.8	88.7	36.7	88.7	60.3
	StreamingLLM	61.1	51.8	48.4	76.0	23.2	22.0	15.3	28.7	40.8
	FastV	67.1	53.9	49.2	78.0	14.8	82.7	26.7	71.3	55.5
	Ours	69.7	54.1	48.3	78.2	16.3	89.3	41.3	89.3	60.8

Table 1. The overall performance comparison across different models and methods on VideoMME, NextQA, and VideoNIAH benchmarks. All token compression methods employ 30% relative token budget.

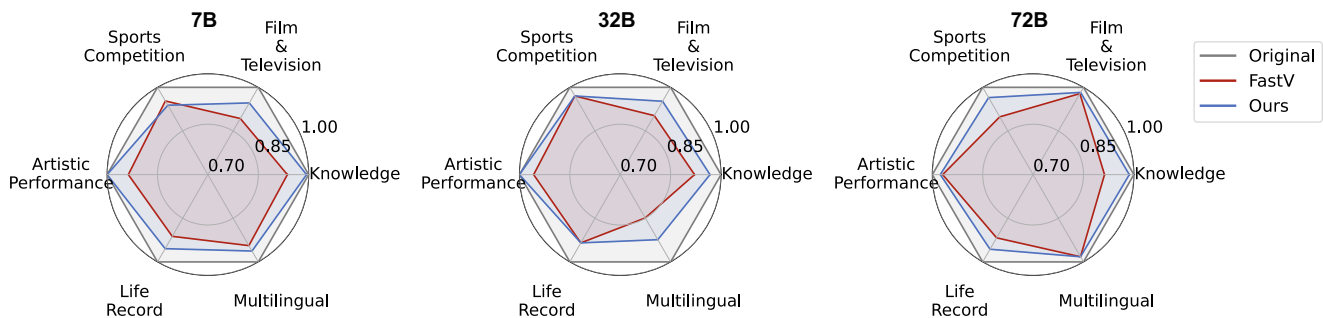


Figure 9. The VideoMME performance for each category across Llava-Video-7B, 32B, and 72B for different methods. All scores are normalized by the original model.

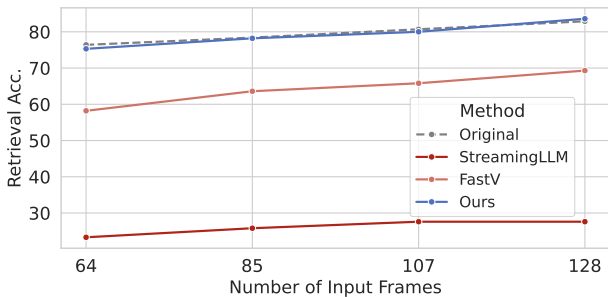


Figure 10. The VideoNIAH performance for the Llava-Video-7B across various numbers of input frames.

model family. As shown in Figure 13, FrameFusion consistently outperforms FastV baseline across all model sizes and VideoMME categories, demonstrating comparative performance with the original model at a 30% relative token budget. The numeric results are shown in Appendix 8.5.

Scaling Input Length. Figure 10 shows that FrameFusion surpass other baselines to achieve high retrieval accuracies across diverse input number of frames, demonstrating comparable performance with the original dense model. Fig-

ure 8 shows increasing LLM speedups and memory reductions with more input frames.

5.6. Ablation Study

We validate the impact of each observation and design choice in FrameFusion, demonstrating their individual effectiveness in this section.

Design Choice 1. Instead of computing $N \times N$ token similarities with significant overhead, FrameFusion calculates N token similarities only between corresponding vision tokens in adjacent frames. We compare our approach with two common alternatives: 1. *The adjacent strategy*, which computes N similarities between adjacent image patches (i.e., adjacent vision tokens). 2. *The random strategy*, which calculates similarities for N randomly selected token pairs. All three strategies are compared against the posterior optimal upper bound, which merges the most similar tokens using the full $N \times N$ similarity computation. As shown in Figure 11, we evaluate the top-K hit number for each strategy. This metric indicates how many of the top-k similar token pairs identified by a given strategy align with those selected by the posterior optimal approach. For visualization clarity, we limit the number of frames to three

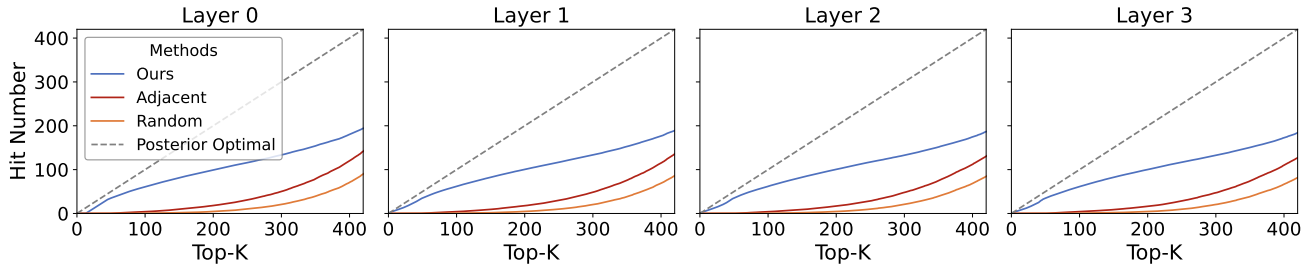


Figure 11. Top-k hit numbers for different similarity calculation strategies on the initial layers of the Llava-Video-7B model.

Merging Layer	Budget	Merging Rate	Retrieval Acc.
Original	100%	0%	76.4%
0	50%	50.0%	76.2%
1	50%	52.0%	76.8%
2	50%	53.8%	76.4%
12	50%	87.5%	74.4%
13	50%	93.3%	64.2%
14	50%	100.0%	48.9%

Table 2. Performance on VideoNIAH of different merging layers with the same relative token budget of 50%.

Method	VideoMME \uparrow	VideoNIAH \uparrow
Original	63.2	76.4
Prune then merge	59.9	73.1
Merge then prune	60.9	73.3

Table 3. Performance of the Llava-Video-7B model of different orders between merging and pruning.

(420 non-first-frame vision tokens) from each video. Our method consistently outperforms the adjacent and random strategies across all model layers.

Design Choice 2. FrameFusion first merges at the initial layers, then prunes at subsequent layers. We validate the influence of the merging layer position. As shown in Table 2, given the same token reduction budget, merging at shallow layers shows significantly better performance than merging at deeper layers. Additionally, we examine the effect of the order of merging and pruning. As shown in Table 3, with a fixed token budget of $C = 0.3$ and the same number of tokens reduced in layers 1 and 2, merging before pruning achieves better performance compared to pruning before merging.

Design Choice 3. FrameFusion adopts a cascaded merging strategy, where merged tokens remain reduced across layers to maximize efficiency. To evaluate the accuracy-efficiency trade-offs of cascaded merging, we use non-cascaded merging

	\approx Budget	VideoNIAH \uparrow	
#Frame	w. Cascaded	Original	Ours (Cascaded)
8	92.8%	20.0	20.7
16	90.0%	29.1	28.0
32	81.5%	43.8	42.9
64	72.2%	76.4	75.6

Table 4. Equivalent relative token budgets and VideoNIAH scores of cascaded merging across different numbers of frames, aligned to the minimum FLOPs achievable by non-cascaded merging.

ing (KV-cache merging) as a baseline. This baseline reduces only the computation of attention matrices while leaving FFN computations unchanged. We calculate the minimum FLOPs achievable with non-cascaded merging by removing all KV-caches. As shown in Table 4, under the same FLOPs, FrameFusion requires token budgets of only 72% to 93% when using cascaded pruning—substantially more relaxed than the 30% budgets used in the main experiments. Across different numbers of frames, FrameFusion achieves performance comparable to the original model, while the non-cascaded model will fail due to the absence of KV-caches.

6. Conclusion

In this paper, we propose FrameFusion, a similarity-based token merging method for video LLMs. By combining similarity-based merging with importance-based pruning, FrameFusion reduces redundant visual tokens while retaining critical information. This approach optimizes computational efficiency and memory usage, enabling accurate video understanding with significantly fewer tokens. Experiments across multiple benchmarks demonstrate a 70% reduction in vision tokens with minimal performance loss, achieving over $3.1\times$ LLM speedups and $1.6\times$ end-to-end speedups. FrameFusion providing new insights in token similarity for LLMs, offering an efficient and scalable solution for real-world video language applications.

References

- [1] Zefan Cai, Yichi Zhang, Bofei Gao, Yuliang Liu, Tianyu Liu, Keming Lu, Wayne Xiong, Yue Dong, Baobao Chang, Junjie Hu, et al. Pyramidkv: Dynamic kv cache compression based on pyramidal information funneling. *arXiv preprint arXiv:2406.02069*, 2024. 5
- [2] Liang Chen, Haozhe Zhao, Tianyu Liu, Shuai Bai, Junyang Lin, Chang Zhou, and Baobao Chang. An image is worth 1/2 tokens after layer 2: Plug-and-play inference acceleration for large vision-language models, 2024. 2, 3, 4, 5, 1
- [3] Xuanyao Chen, Zhijian Liu, Haotian Tang, Li Yi, Hang Zhao, and Song Han. Sparsevit: Revisiting activation sparsity for efficient high-resolution vision transformer. In *Proceedings of the IEEE/CVF Conference on Computer Vision and Pattern Recognition*, pages 2061–2070, 2023. 1
- [4] Zhe Chen, Jiannan Wu, Wenhai Wang, Weijie Su, Guo Chen, Sen Xing, Muyan Zhong, Qinglong Zhang, Xizhou Zhu, Lewei Lu, et al. Intervl: Scaling up vision foundation models and aligning for generic visual-linguistic tasks. In *Proceedings of the IEEE/CVF Conference on Computer Vision and Pattern Recognition*, pages 24185–24198, 2024. 1, 2
- [5] Xiaoyi Dong, Pan Zhang, Yuhang Zang, Yuhang Cao, Bin Wang, Linke Ouyang, Songyang Zhang, Haodong Duan, Wenwei Zhang, Yining Li, et al. Internlm-xcomposer2-4khd: A pioneering large vision-language model handling resolutions from 336 pixels to 4k hd. *arXiv preprint arXiv:2404.06512*, 2024. 2
- [6] Chaoyou Fu, Yuhan Dai, Yondong Luo, Lei Li, Shuhuai Ren, Renrui Zhang, Zihan Wang, Chenyu Zhou, Yunhang Shen, Mengdan Zhang, et al. Video-mme: The first-ever comprehensive evaluation benchmark of multi-modal llms in video analysis. *arXiv preprint arXiv:2405.21075*, 2024. 2, 6
- [7] Qichen Fu, Minsik Cho, Thomas Merth, Sachin Mehta, Mohammad Rastegari, and Mahyar Najibi. Lazyllm: Dynamic token pruning for efficient long context llm inference. *arXiv preprint arXiv:2407.14057*, 2024. 1
- [8] Tianyu Fu, Haofeng Huang, Xuefei Ning, Genghan Zhang, Boju Chen, Tianqi Wu, Hongyi Wang, Zixiao Huang, Shiyao Li, Shengen Yan, et al. Moa: Mixture of sparse attention for automatic large language model compression. *arXiv preprint arXiv:2406.14909*, 2024. 2, 4, 5
- [9] Suyu Ge, Yunan Zhang, Liyuan Liu, Minjia Zhang, Jiawei Han, and Jianfeng Gao. Model tells you what to discard: Adaptive kv cache compression for llms. *ArXiv*, abs/2310.01801, 2023. 2
- [10] Chi Han, Qifan Wang, Wenhan Xiong, Yu Chen, Heng Ji, and Sinong Wang. Lm-infinite: Simple on-the-fly length generalization for large language models. *arXiv preprint arXiv:2308.16137*, 2023. 2
- [11] Bo He, Hengduo Li, Young Kyun Jang, Menglin Jia, Xuefei Cao, Ashish Shah, Abhinav Shrivastava, and Ser-Nam Lim. Ma-lmm: Memory-augmented large multimodal model for long-term video understanding. In *Proceedings of the IEEE/CVF Conference on Computer Vision and Pattern Recognition*, pages 13504–13514, 2024. 2
- [12] Huiqiang Jiang, Yucheng Li, Chengruidong Zhang, Qianhui Wu, Xufang Luo, Surin Ahn, Zhenhua Han, Amir H Abdi, Dongsheng Li, Chin-Yew Lin, et al. Minference 1.0: Accelerating pre-filling for long-context llms via dynamic sparse attention. *arXiv preprint arXiv:2407.02490*, 2024. 2
- [13] Yizhang Jin, Jian Li, Yexin Liu, Tianjun Gu, Kai Wu, Zhengkai Jiang, Muyang He, Bo Zhao, Xin Tan, Zhenye Gan, et al. Efficient multimodal large language models: A survey. *arXiv preprint arXiv:2405.10739*, 2024. 2
- [14] Bo Li, Yuanhan Zhang, Dong Guo, Renrui Zhang, Feng Li, Hao Zhang, Kaichen Zhang, Yanwei Li, Ziwei Liu, and Chunyuan Li. Llava-onevision: Easy visual task transfer. *arXiv preprint arXiv:2408.03326*, 2024. 1, 2
- [15] Junnan Li, Dongxu Li, Silvio Savarese, and Steven Hoi. Blip-2: Bootstrapping language-image pre-training with frozen image encoders and large language models. In *International conference on machine learning*, pages 19730–19742. PMLR, 2023. 4
- [16] Junyan Li, Delin Chen, Tianle Cai, Peihao Chen, Yining Hong, Zhenfang Chen, Yikang Shen, and Chuang Gan. Flex-attention for efficient high-resolution vision-language models. In *European Conference on Computer Vision*, pages 286–302. Springer, 2025. 2
- [17] Yuhong Li, Yingbing Huang, Bowen Yang, Bharat Venkitesh, Acyr Locatelli, Hanchen Ye, Tianle Cai, Patrick Lewis, and Deming Chen. Snapkv: Llm knows what you are looking for before generation. *arXiv preprint arXiv:2404.14469*, 2024. 4
- [18] Yanwei Li, Chengyao Wang, and Jiaya Jia. Llama-vid: An image is worth 2 tokens in large language models. In *European Conference on Computer Vision*, pages 323–340. Springer, 2025. 1, 2
- [19] Zichang Liu, Aditya Desai, Fangshuo Liao, Weitao Wang, Victor Xie, Zhaozhuo Xu, Anastasios Kyrillidis, and Anshumali Shrivastava. Scissorhands: Exploiting the persistence of importance hypothesis for llm kv cache compression at test time. *ArXiv*, abs/2305.17118, 2023. 2
- [20] Jiaming Tang, Yilong Zhao, Kan Zhu, Guangxuan Xiao, Baris Kasikci, and Song Han. Quest: Query-aware sparsity for efficient long-context llm inference. *arXiv preprint arXiv:2406.10774*, 2024. 4
- [21] Gemini Team, Petko Georgiev, Ving Ian Lei, Ryan Burnell, Libin Bai, Anmol Gulati, Garrett Tanzer, Damien Vincent, Zhufeng Pan, Shibo Wang, et al. Gemini 1.5: Unlocking multimodal understanding across millions of tokens of context. *arXiv preprint arXiv:2403.05530*, 2024. 1, 2
- [22] Dezhao Tu, Danylo Vashchilenko, Yuzhe Lu, and Panpan Xu. Vl-cache: Sparsity and modality-aware kv cache compression for vision-language model inference acceleration. *arXiv preprint arXiv:2410.23317*, 2024. 2
- [23] Hanrui Wang, Zhekai Zhang, and Song Han. Spatten: Efficient sparse attention architecture with cascade token and head pruning. *2021 IEEE International Symposium on High-Performance Computer Architecture (HPCA)*, pages 97–110, 2020. 1, 4
- [24] Yuetian Weng, Mingfei Han, Haoyu He, Xiaojun Chang, and Bohan Zhuang. Longvlm: Efficient long video understanding via large language models. In *European Conference on Computer Vision*, pages 453–470. Springer, 2025. 1, 2

- [25] Wenhao Wu, Yizhong Wang, Guangxuan Xiao, Hao Peng, and Yao Fu. Retrieval head mechanistically explains long-context factuality. *arXiv preprint arXiv:2404.15574*, 2024. [4](#)
- [26] Guangxuan Xiao, Yuandong Tian, Beidi Chen, Song Han, and Mike Lewis. Efficient streaming language models with attention sinks. *The Twelfth International Conference on Learning Representations*, 2024. [2](#), [5](#), [1](#)
- [27] Junbin Xiao, Xindi Shang, Angela Yao, and Tat-Seng Chua. Next-qa: Next phase of question-answering to explaining temporal actions. In *Proceedings of the IEEE/CVF Conference on Computer Vision and Pattern Recognition (CVPR)*, pages 9777–9786, 2021. [6](#)
- [28] Mingze Xu, Mingfei Gao, Zhe Gan, Hong-You Chen, Zhengfeng Lai, Haiming Gang, Kai Kang, and Afshin Dehghan. Slowfast-llava: A strong training-free baseline for video large language models. *arXiv preprint arXiv:2407.15841*, 2024. [2](#)
- [29] Yuan Yao, Tianyu Yu, Ao Zhang, Chongyi Wang, Junbo Cui, Hongji Zhu, Tianchi Cai, Haoyu Li, Weilin Zhao, Zhihui He, et al. Minicpm-v: A gpt-4v level mllm on your phone. *arXiv preprint arXiv:2408.01800*, 2024. [1](#), [2](#), [6](#), [4](#)
- [30] Jerrold H Zar. Spearman rank correlation. *Encyclopedia of biostatistics*, 7, 2005. [4](#)
- [31] Junyang Zhang, Mu Yuan, Ruiguang Zhong, Puhao Luo, Huiyou Zhan, Ningkang Zhang, Chengchen Hu, and Xiangyang Li. A-vl: Adaptive attention for large vision-language models. *arXiv preprint arXiv:2409.14846*, 2024. [2](#)
- [32] Kaichen Zhang, Bo Li, Peiyuan Zhang, Fanyi Pu, Joshua Adrian Cahyono, Kairui Hu, Shuai Liu, Yuanhan Zhang, Jingkang Yang, Chunyuan Li, and Ziwei Liu. Lmms-eval: Reality check on the evaluation of large multimodal models, 2024. [6](#)
- [33] Yuan Zhang, Chun-Kai Fan, Junpeng Ma, Wenzhao Zheng, Tao Huang, Kuan Cheng, Denis Gudovskiy, Tomoyuki Okuno, Yohei Nakata, Kurt Keutzer, et al. Sparsevlm: Visual token sparsification for efficient vision-language model inference. *arXiv preprint arXiv:2410.04417*, 2024. [2](#)
- [34] Yuanhan Zhang, Jinming Wu, Wei Li, Bo Li, Zejun Ma, Ziwei Liu, and Chunyuan Li. Video instruction tuning with synthetic data. *arXiv preprint arXiv:2410.02713*, 2024. [1](#), [2](#), [6](#)
- [35] Zhenyu (Allen) Zhang, Ying Sheng, Tianyi Zhou, Tianlong Chen, Lianmin Zheng, Ruisi Cai, Zhao Song, Yuandong Tian, Christopher Ré, Clark W. Barrett, Zhangyang Wang, and Beidi Chen. H2o: Heavy-hitter oracle for efficient generative inference of large language models. *ArXiv*, abs/2306.14048, 2023. [1](#), [2](#), [4](#)
- [36] Zijia Zhao, Haoyu Lu, Yuqi Huo, Yifan Du, Tongtian Yue, Longteng Guo, Bingning Wang, Weipeng Chen, and Jing Liu. Needle in a video haystack: A scalable synthetic framework for benchmarking video mllms. *arXiv preprint arXiv:2406.09367*, 2024. [6](#)

FrameFusion: Combining Similarity and Importance for Video Token Reduction on Large Visual Language Models

Supplementary Material

7. Detailed Experiment Setup

For the baselines StreamingLLM [26] and FastV [2], we follow the official implementations and set the attention sink size of StreamingLLM to 8 and K in FastV to 2.

For FrameFusion, the merging ratios across layers are controlled by two hyperparameters: $S_{\text{threshold}}$ and $N_{\text{threshold}}$, as discussed in Section 4.1.

$S_{\text{threshold}}$ defines the minimum cosine similarity required for two tokens to be considered similar and merged. Since similarity distributions vary across models, we set $S_{\text{threshold}}$ to match the median of similarity at the first model layer under typical input cases, such as 128 samples from the VideoMME dataset. For the Llava-Video series, we set $S_{\text{threshold}} = 0.6$; while for MiniCPM-V, we set $S_{\text{threshold}} = 0.7$.

$N_{\text{threshold}}$ determines the transition from merging to pruning. If the number of similar tokens (tokens with cosine similarity above $S_{\text{threshold}}$) falls below $N_{\text{threshold}}$, the model switches to pruning. We set $N_{\text{threshold}} = 0.1$ to avoid extensive similarity computations across the entire model.

To ensure the merging process does not excessively reduce the token count below the predefined token budget C , we precompute the maximum number of token pairs (N_{max}) that can be merged per layer. If the actual number of pairs exceeds N_{max} , only the top N_{max} pairs with the highest cosine similarity are merged. Any remaining merging or pruning steps are skipped, and the model proceeds with a standard forward pass.

8. Additional Experiment Results

8.1. Performance Across Token Budgets

Table 5 presents the benchmark performance of the Llava-Video-7B model at token budgets ranging from 0.3 to 0.7. At a 30% token budget, FrameFusion achieves strong performance, with a maximum relative drop of less than 3.0% compared to the dense model. As the budget increases to 0.5 and 0.7, the maximum drops further decrease to $\leq 1.2\%$.

8.2. Retrieval Analysis

We further investigate the retrieval accuracy details with the VideoNIAH benchmark, as shown in Figure 12. FrameFusion demonstrates similar retrieval performance as the original dense model, with consistent performance across lengths and positions. In contrast, StreamingLLM hardly retrieves the initial frames of the video. FastV does not

show particular failure patterns but undergoes uniform performance degradation across grids.

8.3. Speedup Across Model Sizes

We evaluate the scalability of FrameFusion’s speedup across different model sizes, as shown in Figure 13. To accommodate the increased KV-Cache and memory overhead, we distribute the models across multiple GPUs. With larger models, FrameFusion achieves greater end-to-end speedups, delivering $2.8\times$ for Llava-Video-32B on two GPUs and $3.2\times$ for Llava-Video-72B on four GPUs at a 30% token budget.

8.4. Token Reduction Details

FrameFusion reduces computational cost through both token merging and pruning. Using 128 samples from the VideoMME dataset with the Llava-Video-7B model, we calculate the token count per layer. As shown in Figure 14, FrameFusion progressively reduces tokens per layer, achieving the desired relative token budget (represented by the area under the line).

8.5. Scalability Numeric Results

We present the detailed numeric results of the scalability experiments in Section 5.5.

Table 6 provides the VideoMME scores for various model sizes across different video categories, offering a numerical breakdown of Figure 13. FrameFusion consistently outperforms the baseline methods across diverse model sizes and video categories.

Table 7 illustrates how retrieval accuracy scales with the number of input frames, complementing the insights from Figure 10. As shown, FrameFusion maintains consistent accuracy improvements across increasing frame numbers, matching the performance of the original model. In contrast, both StreamingLLM and FastV exhibit noticeable drops in accuracy.

9. Asymptotic Complexity Analysis

We estimate the computing cost of FrameFusion following the approach of FastV [2]. Given a model with L layers and a specified relative token budget C , FrameFusion operates in the merging stage from layer 0 to layer $K - 1$, then transitions to the pruning stage at layer K . Let N_l denote the number of tokens layer l before token reduction at this layer. Note that N_{l+1} represents the number of tokens of layer l

Model	Method	Budget	VideoMME		NExt-QA-MC		NExt-QA-OE		Max. Drop ↓
			Score ↑	Drop ↓	Score ↑	Drop ↓	Score ↑	Drop ↓	
Llava-Video-7B	Original	1.0	63.2	-	83.2	-	32.1	-	-
	Ours	0.3	61.3	3.0%	81.8	1.7%	31.7	1.2%	3.0%
		0.5	62.6	0.9%	82.7	0.6%	32.1	0.0%	0.9%
		0.7	63.0	0.3%	82.8	0.5%	32.1	0.0%	0.5%
MiniCPM-V-8B	Original	1.0	58.5	-	78.9	-	13.8	-	-
	Ours	0.3	57.4	1.9%	78.2	0.9%	16.3	-18.1%	1.9%
		0.5	58.5	0.0%	78.6	0.4%	17.4	-26.1%	0.4%
		0.7	57.8	1.2%	78.6	0.4%	16.1	-16.7%	1.2%

Table 5. Performance comparison between the original and proposed methods on VideoMME, NExt-QA-MC, and NExt-QA-OE benchmarks with different relative token budgets on Llava-Video-7B model. Drop indicates the relative performance decrease compared to the original method.

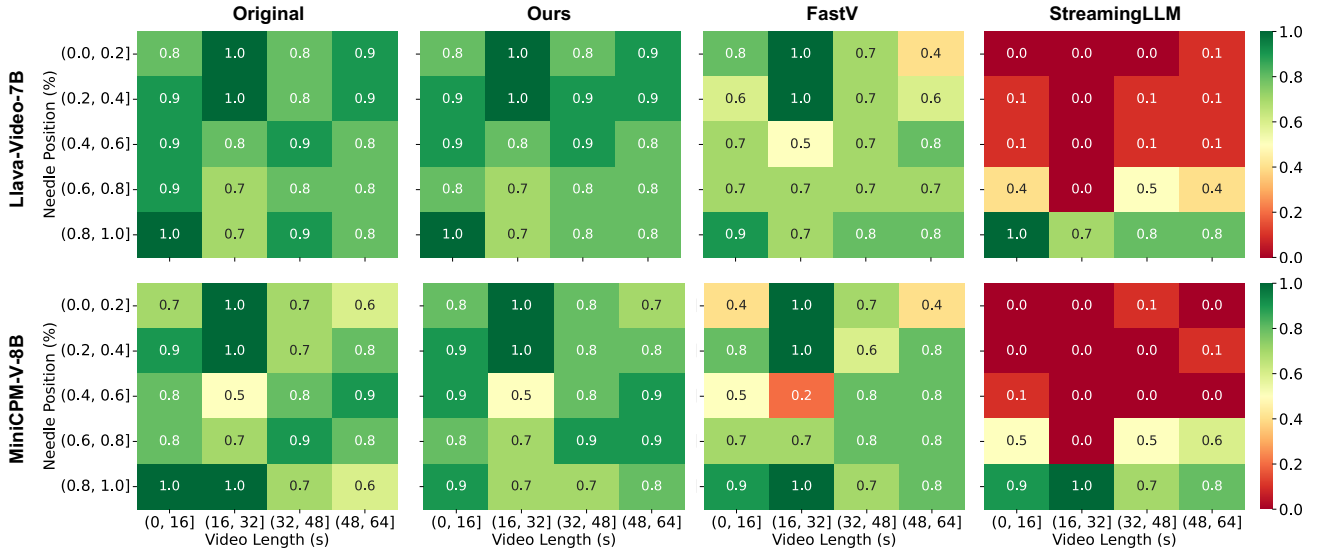


Figure 12. VideoNIAH retrieval accuracy of the Llava-Video-7B and MiniCPM-V-8B models using different token compression methods across varying video lengths and retrieval positions. All token compression methods employ 30% relative token budget.

after token reduction, and we let N_{-1} equal the original input token length N . FrameFusion reduces N_l with merging and pruning at the initial $K + 1$ layers. After the token reduction, the remaining tokens for the successive layers are calculated as follows:

$$N_l = \frac{L \times C \times N - (N_0 + \dots + N_K)}{L - K - 1}, l \in [K + 1, L] \quad (4)$$

The model inference computation FLOPs $F(N_l, N_{l+1})$ of layer l is calculated as follows:

$$F(N_l, N_{l+1}) = 4N_l D^2 + 2N_l^2 D + 3N_{l+1} D M \quad (5)$$

where D denotes the hidden state size, and M denotes the intermediate FFN size. The additional computation $F'(N_l)$

introduced by FrameFusion during similarity computation is:

$$F'(N_l) = 3N_l D \quad (6)$$

Note that the additional computation F' introduced by FrameFusion shows neglectable asymptotic complexity with respect to input length and model size, comparing with the $O(N^2 D)$ and $O(N D^2)$ complexities of the original model.

10. Additional Observation Details

10.1. Similarity Distribution Details

We take 128 videos from the VideoMME dataset and calculate the variance in token similarity across different layers.

Model	Method	Knowledge	Film & Television	Sports Competition	Artistic Performance	Life Record	Multilingual
Llava-Video-7B	Original	63.1	67.2	61.8	61.7	63.7	58.9
	StreamingLLM	55.1	57.2	56.0	54.2	52.9	48.9
	FastV	59.1	60.0	58.9	57.8	58.1	55.6
	Ours	62.7	63.6	58.0	61.7	60.8	56.7
Llava-Video-32B	Original	60.9	68.9	57.3	59.2	58.1	58.9
	StreamingLLM	53.1	55.6	50.2	53.3	49.5	53.3
	FastV	56.1	62.2	55.6	56.7	54.3	50.0
	Ours	58.9	65.6	55.6	59.2	54.3	54.4
Llava-Video-72B	Original	73.2	74.4	68.0	71.4	68.9	62.2
	StreamingLLM	65.7	66.7	59.3	65.6	58.7	58.9
	FastV	66.8	72.8	61.1	69.2	63.2	61.1
	Ours	72.2	73.1	65.6	69.7	65.9	61.1

Table 6. Numeric VideoMME scores of different methods and model sizes across various video categories.

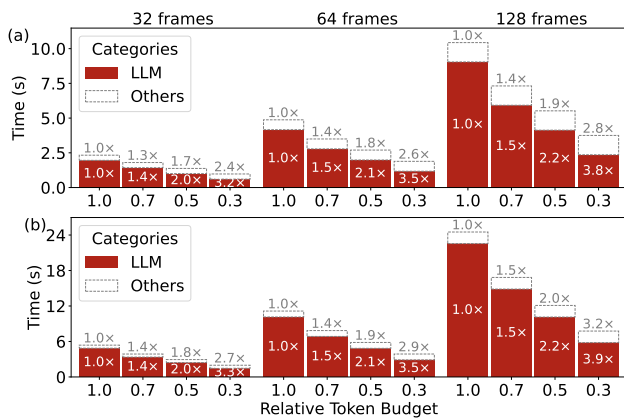


Figure 13. Runtime of (a) Llava-Video-32B on two A100-80GB GPUs and (b) Llava-Video-72B on four A100-80GB GPUs using FrameFusion. Numbers on bars indicate LLM and end-to-end speedups.

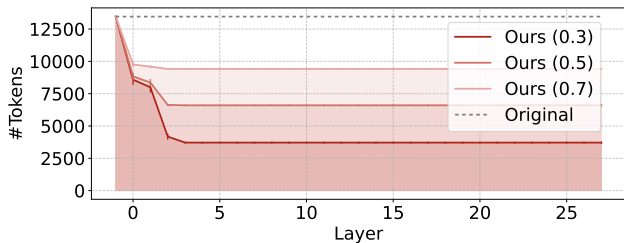


Figure 14. Average number of tokens per layer in the Llava-Video-7B model with FrameFusion at different relative token budgets. Error bars represent variance across data items.

Method	Number of frames				Max. Relative Drop
	64	85	107	128	
Original	76.4	78.4	80.7	82.9	-
StreamingLLM	23.3	25.8	27.6	27.6	70%
FastV	58.2	63.6	65.8	69.3	24%
Ours	75.3	78.2	80.0	83.6	1%

Table 7. Numeric VideoNIAH retrieval accuracy of different methods across various frame counts.

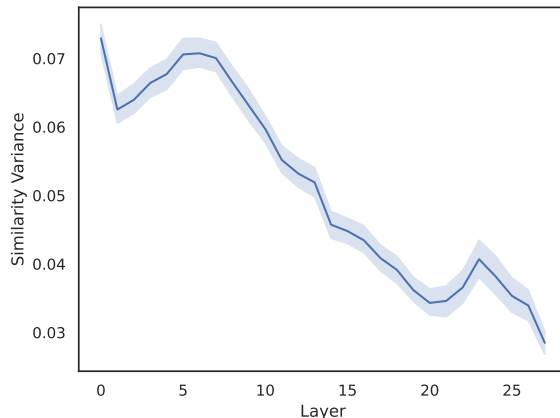


Figure 15. Average token similarity variance per LLM layer in the Llava-Video-7B model, tested on 128 samples from the VideoMME dataset. Shading represents the variance across data items.

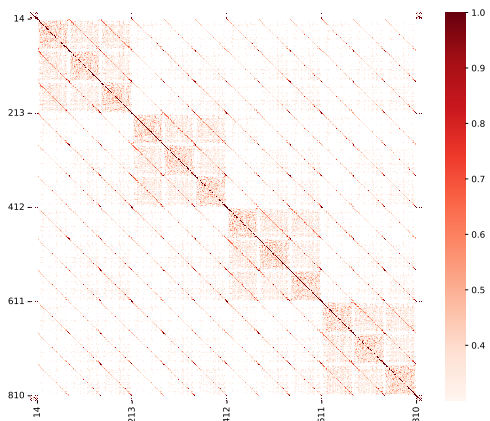


Figure 16. Token similarities between all input tokens at the first LVLN layer in MiniCPM-V-8B.

As shown in Figure 15, the similarity variance decreases in the deeper layers of the model, validating Observation 2.

10.2. Observations on Additional Models

In addition to the analysis of the Llava-Video model in Section 3, we conduct a similar study on the MiniCPM architecture. Results are presented in Figures 16, 17, 18, and 19.

Overall, the conclusions align with those of the Llava-Video model, with a few notable differences: Firstly, as shown in Figure 16, MiniCPM, which incorporates Q-Former [15, 29], exhibits additional high similarity among vision tokens within the same frame. However, the prominent 210th sub-diagonal persists, supporting our token similarity calculation strategy. Secondly, as shown in Figure 17, high similarity decreases less steeply in deeper layers for MiniCPM compared to Llava-Video. Despite this, the superior efficiency of cascaded merging at shallower layers ensures that Design Choice 2 remains valid.

10.3. Video Pruning Visualization

We select a video example to visualize the effect of our token merging strategy. Figure 20 shows the frames of the original video sampled at a frame rate of 1 fps. In Figure 21, we present the video input to the model after token merging in Layer 0, where blank patches indicate tokens that have been merged. Furthermore, we replace the blank regions with the average of the merged patches, and the resulting visualization is shown in Figure 22. As shown in the examples, FrameFusion token merging strategy successfully merges similar vision tokens, reducing the computational costs, while maintaining high validity of the video.

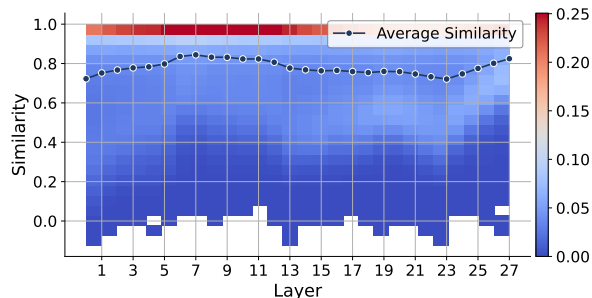


Figure 17. Heatmap of token similarity across different model layers for the MiniCPM-V-8B model. Each cell represents the similarity at a specific layer, with color intensity denoting distribution frequency. The line overlay shows the average token similarity across layers.

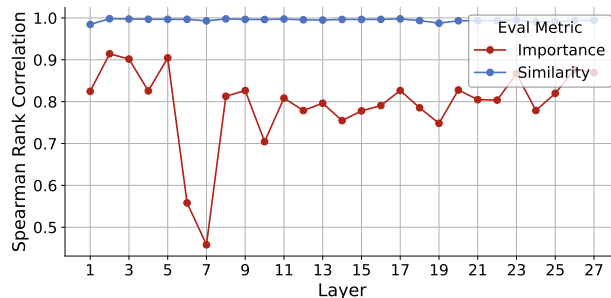


Figure 18. Spearman Rank Correlation between adjacent layers for the MiniCPM-V-8B model.

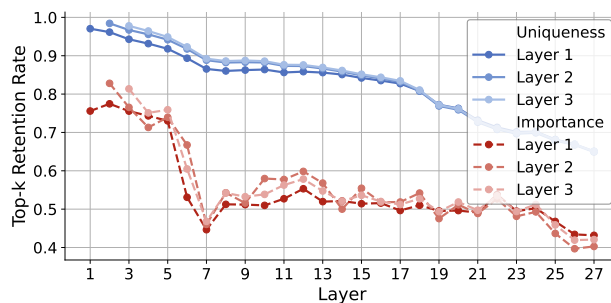


Figure 19. The Top-30% retention rate across model layers for the MiniCPM-V-8B model, using different retention metrics and reference layers.

10.4. Importance-Similarity Joint-Distribution

We visualize the joint distribution of token importance and similarity across different layers of Llava-Video-7B. As shown in Figure 23, it can be observed that in the shallow layers of the model, a significant number of tokens exhibit both high similarity and high importance values. FrameFusion can effectively compress these tokens. This phenomenon becomes less apparent in the deeper layers of the

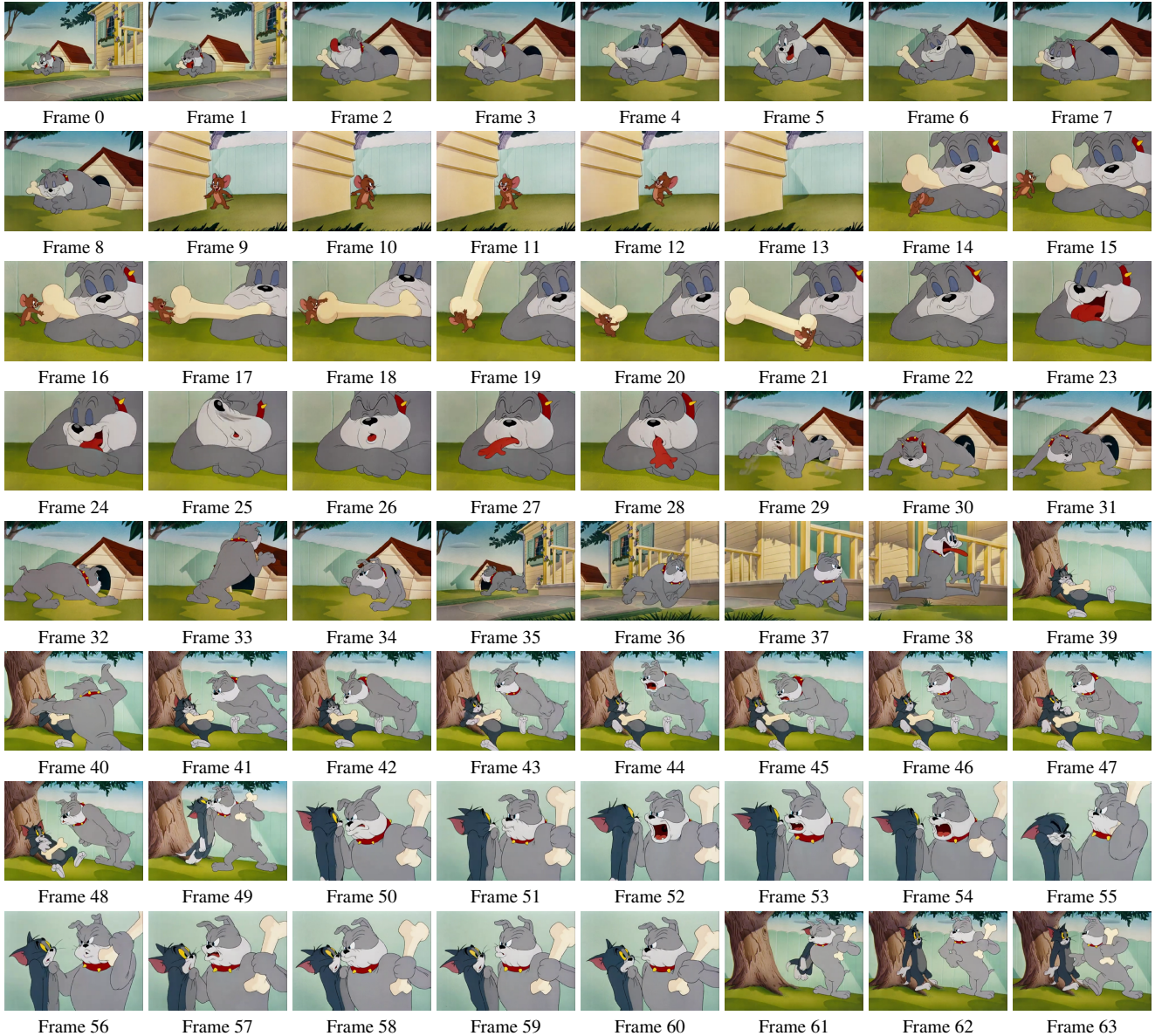


Figure 20. An example input video with 1 fps frame rate.

model, supporting our design choice of performing token merging in the shallow layers of the model.

11. Limitation and Future Works

While FrameFusion demonstrates significant improvements in token reduction and efficiency for video LLMs, certain challenges remain for future works. First, the similarity-based merging process can be further refined to better handle highly diverse or complex video content, minimizing potential information loss. Second, the reliance on pre-defined similarity and importance metrics calls for the development of adaptive and task-specific strategies to im-

prove generalization across diverse scenarios. Future work will focus on designing more robust similarity measures and integrating FrameFusion with advanced token-efficient architectures.

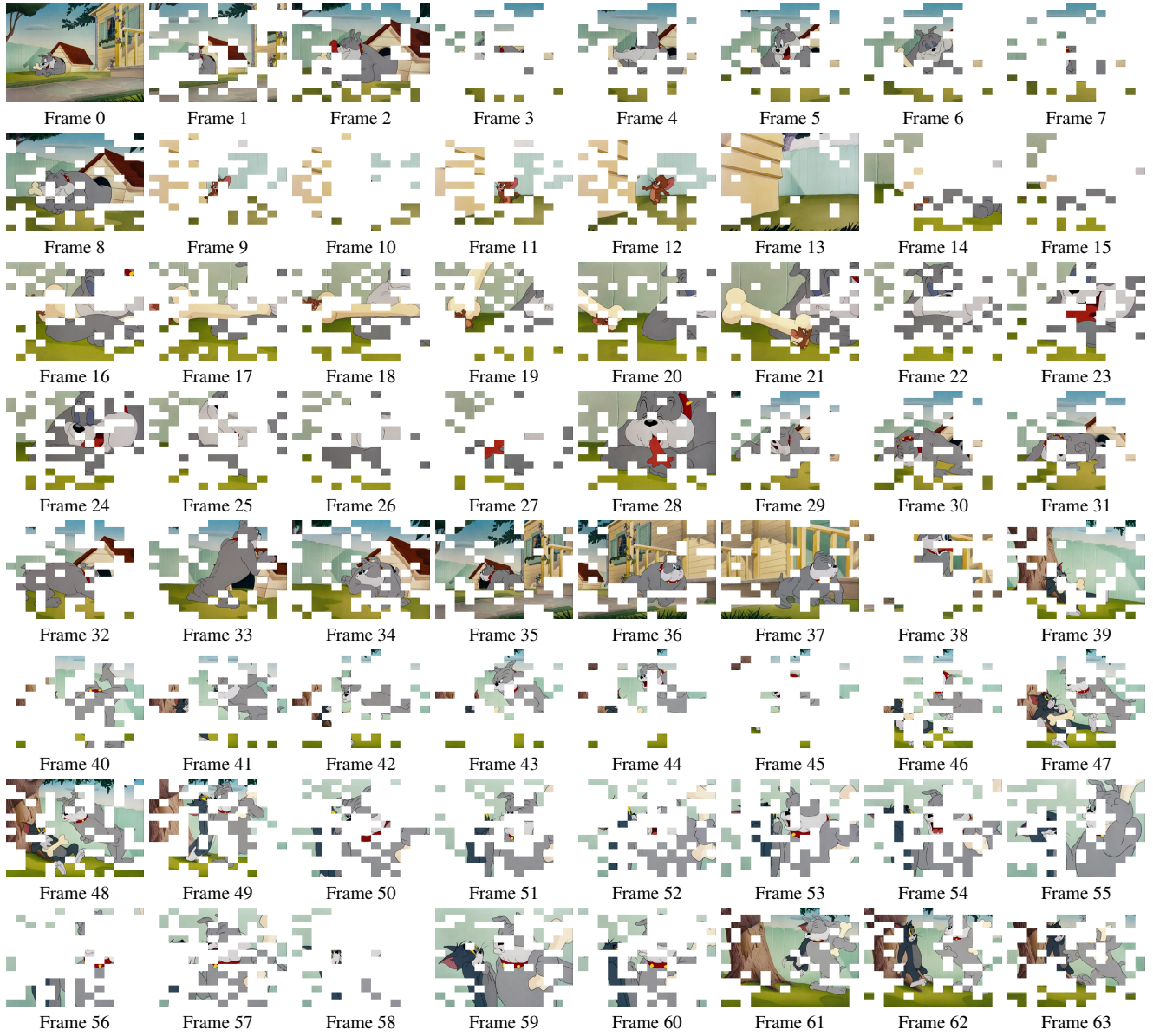


Figure 21. The example of the video after token merging. Merged tokens are visualized with the blank blocks.

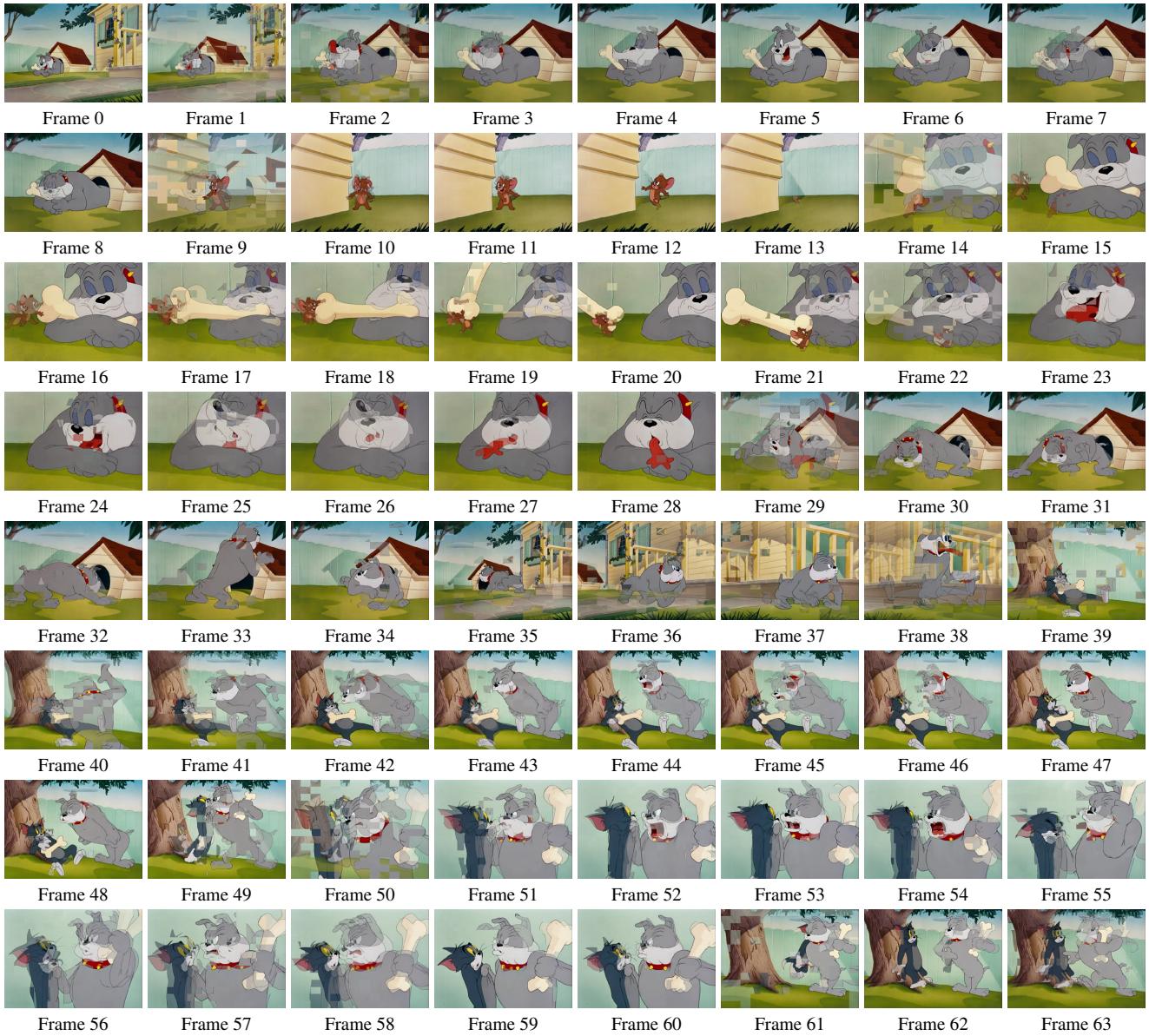


Figure 22. The example of the video after token merging. Merged tokens are visualized with the average image patches.

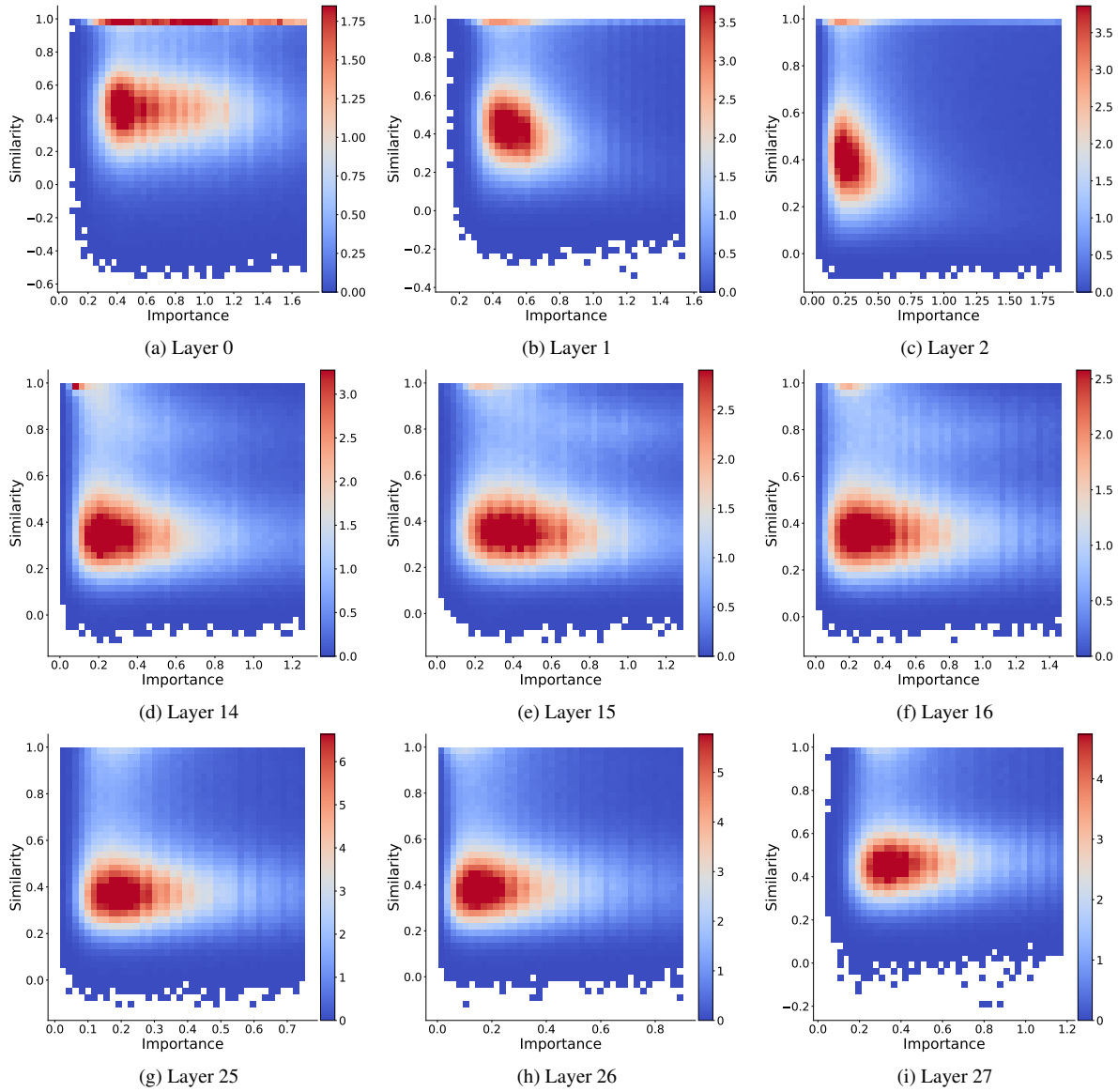


Figure 23. Importance-similarity joint-distribution of different layers, with color intensity denoting distribution frequency.